Theor Chem Acc (2012) 131:1083
DOI 10.1007/s00214-011-1083-9

REGULAR ARTICLE

Calculation of the zero-point energy from imaginary-time quantum trajectory dynamics in Cartesian coordinates

Sophya Garashchuk

Received: 6 July 2011 / Accepted: 19 August 2011 / Published online: 11 January 2012

Abstract The imaginary-time quantum dynamics is implemented in Cartesian coordinates using the momentum-dependent quantum potential approach. A nodeless wavefunction, represented in terms of quantum trajectories, is evolved in imaginary time according to the quantum-mechanical Boltzmann operator in the Eulerian frame-of-reference. The quantum potential and its gradient are determined approximately, from the global low-order (quadratic) polynomial fit to the trajectory momenta, which makes the approach practical in high dimensions. Implementation in the Cartesian coordinates allows one to work with the Hamiltonian of the simplest form, to setup calculations in the molecular dynamics-compatible framework and to naturally mix quantum and classical description of particles. Localization of wavefunctions in the center-of-mass degrees of freedom and in the overall rotation, which makes the quadratic polynomial fitting in Cartesian coordinates accurate, is accomplished by the addition of a quadratic constraining potential, and its contribution to the zero-point energy is analytically subtracted. For illustration, the zero-point energies are computed for model clusters consisting of up to 11 atoms (33 dimensions).

Keywords Quantum dynamics · Quantum trajectories · Zero-point energy · Boltzmann operator · Imaginary time

Published as part of the special collection of articles celebrating the 50th anniversary of Theoretical Chemistry Accounts/Theoretica Chimica Acta.

S. Garashchuk (✉)
Department of Chemistry and Biochemistry,
University of South Carolina, Columbia, SC 29208, USA
e-mail: sgarashc@mail.chem.sc.edu

1 Introduction

The quantum-mechanical (QM) behavior of nuclei, manifested in the zero-point energy (ZPE) effect, tunneling and nonadiabatic transitions, is often essential for accurate description and understanding of reactions in gas phase and complex chemical environments, especially in processes involving hydrogen at low temperatures and energies. For example, ZPE stored in the vibrational modes of chemical reactants, products and transition-state species modifies reaction energy barriers, which can greatly influence the reaction rates and branching ratios [1, 2]. QM tunneling can be critical in proton transfer reactions [3–6]. Nonadiabatic dynamics involving transitions between different electronic or vibrational energy levels is always present in photochemistry [7–9]. As the system size increases, it becomes very difficult to describe molecular systems quantum-mechanically due to the exponential scaling of the standard methods of solving the time-dependent Schrödinger equation [10]. A number of multidimensional quantum approaches have been developed over the years, including those using basis contractions [11–13], Gaussian coherent state representations [14, 15] and mixed quantum/classical strategies [16–22]. Nevertheless, since 2001, up to date reaction dynamics of hydrogen and methane remains the largest reactive scattering process studied quantum-mechanically in full dimension using exact evolution method, the Multi-Configurational Time-Dependent Hartree method [12, 23].

At the same time, the classical treatment of nuclei is often appropriate, and the simulation methods based on classical trajectory dynamics [24] are applicable to molecular systems comprised of thousands of atoms. The trajectory representation of large molecular systems is appealing for several reasons. One reason is that the trajectory description of heavy particles, based on quasiclassical, semiclassical or quantum

trajectory dynamics, is often more appropriate than the grid or basis representation, because close to the classical limit, $\hbar \to 0$, the wavefunctions are highly oscillatory. Another reason is that the initial conditions for the trajectories simulation can be chosen randomly, which formally circumvents the exponential scaling of the wavefunction representation with the system size. (The conventional direct product grid or basis methods scale exponentially by construction). In general, a wavefunction for an arbitrary coupled anharmonic Hamiltonian will be an exponentially complex object, but for molecular systems with most of the nuclei behaving classically one expects simpler wavefunctions due to quantum and thermal decoherence [25]. Not surprisingly, incorporation of QM effects into classical trajectory framework is a long-standing theoretical goal, which motivated the development of quasiclassical [26] and semiclassical methods (for example see [27]) traditionally based on dynamics of *independent* classical trajectories.

A number of recent trajectory methodologies [28], related to the quantum or the Madelung–de Broglie–Bohm trajectory formulation of the time-dependent Schrödinger equation [29–31], incorporate the intrinsically non-local QM effects into evolution of a trajectory *ensemble* representing a wavefunction. In this paper, we implement an approximate method of this type, namely dynamics with the momentum-dependent quantum potential (MDQP) [32] in Cartesian space: a wavefunction is evolved in imaginary time according to the QM Boltzmann operator yielding the ZPE estimates for high-dimensional systems. Implementation in the Cartesian coordinates is important because it allows one to work with the Hamiltonian of the simplest form, to setup calculations in the molecular dynamics-compatible framework and to naturally mix quantum and classical description of particles. The MDQP and its gradient are determined approximately from the global fit of the trajectory momentum, which is necessary for a practical multidimensional implementation with polynomial scaling. Section 2 describes the formalism and implementation, for simplicity in one dimension; ∇ denotes the spatial derivatives throughout, including the one-dimensional case $\nabla = \partial/\partial x$. Numerical illustration for a model cluster (up to 11 particles) is given in Sect. 3. Section 4 presents discussion and summary.

2 Imaginary-time quantum trajectory evolution in Cartesian coordinates

2.1 The MDQP quantum trajectory formulation in the Eulerian frame-of-reference

The quantum trajectory approach in imaginary time is inspired by the Bohmian formulation of the Schrödinger equation,

$$\hat{H}\psi(x,t) = \mathrm{i}\hbar\frac{\partial}{\partial t}\psi(x,t), \tag{1}$$

with the time-dependent complex wavefunction written in terms of real phase $S(x, t)$ and amplitude $A(x, t)$, $\psi(x,t) = A(x,t)\exp(\mathrm{i}S(x,t)/\hbar)$. This yields the Hamilton–Jacobi equation

$$\frac{\partial S(x,t)}{\partial t} = -\frac{(\nabla S(x,t))^2}{2m} - V - Q \tag{2}$$

and the continuity equation on the probability density $A^2(x,t)$ [31]. Equation 2 leads to the Newtons equations of motion for the trajectories with the momenta $p(x, t) = \nabla S(x, t)$ guided by the sum of the classical potential V and the quantum potential Q,

$$Q = -\frac{\hbar^2}{2m}\frac{\nabla^2 A(x,t)}{A(x,t)}. \tag{3}$$

Exact and approximate implementations of the real-time Bohmian methodology, including applicability and limitations, are reviewed in [28, 33]. The goal of the approximate methodology is to give estimates of the QM effects

The Boltzmann evolution of a wavefunction according to the diffusion equation with the QM Hamiltonian $\hat{H}$,

$$\hat{H}\psi(x,\tau) = -\hbar\frac{\partial}{\partial\tau}\psi(x,\tau), \quad \tau > 0 \tag{4}$$

is equivalent to Eq. 1 with the real-time variable t replaced by $-\imath\tau$. This transformation, the so-called Wick rotation [34], is widely used starting with the path integral formulation of statistical mechanics [35] and including, for example, recent Gaussian-based methods [36–38]. In the semiclassical trajectory context, this transformation generates the real-time trajectory evolution on the inverted classical potential [39].

As $\tau \to \infty$, any initial wavefunction propagated in time according to Eq. 4 will evolve to the lowest energy eigenfunction (of the same symmetry if the system has a definite symmetry), since the lowest energy component is the slowest to decay. Choosing the energy scale so that eigenenergies are positive to avoid the exponential growth of the wavefunction norm $\langle\psi|\psi\rangle_\tau$, the wavefunction energy E will converge to the ZPE value, E_0:

$$E(\tau) = \frac{\langle\psi|\hat{H}|\psi\rangle_\tau}{\langle\psi|\psi\rangle_\tau}, \quad \lim_{\tau\to\infty} E(\tau) = E_0 \tag{5}$$

This feature is central to the Diffusion Monte Carlo methods used in the largest exact QM ZPE calculations [40–44]. The imaginary-time evolution also can be viewed as "cooling" of a system to the temperature T, where $k_B T = 1/\beta = \hbar/\tau$, when acted upon by the Boltzmann operator $\exp(-\beta\hat{H})$ in the thermal reaction rate constant calculations [45].

In MDQP, Eq. 4 is reformulated in terms of trajectories by expressing a nodeless wavefunction as an exponent of the "action" function S, whose gradient is identified with the trajectory momenta [32],

$$p(x,\tau) = \nabla S(x,\tau). \tag{6}$$

We present the formalism for a particle of mass m in one Cartesian dimension x in the Eulerian frame-of-reference. Multidimensional generalizations and the Lagrangian frame-of-reference formulation can be found in [46, 47]; Ref. [48] contains a comparison of the Eulerian and Lagrangian formulations. Equation 4 has been implemented in terms of trajectories earlier by other groups [49, 50] in terms of "independent" quantum trajectories. These methods are based on the hierarchy of differential equations for the high-order gradients of S truncated at a fixed level q ($q = 4$ or 6 in practice); the number of equations scales as $(N_{\mathrm{dim}})^{q+1}$. The MDQP approach evolves only the first derivatives of S, $p = \nabla S$, and the approximation is implemented globally, thus making it practical for high-dimensional systems.

To obtain the classical-like equations of motion, we express a positive wavefunction via a single exponential function,

$$\psi(x,\tau) = \exp\left(-\frac{S(x,\tau)}{\hbar}\right) \tag{7}$$

which, substituted into Eq. 4, gives the equivalent of the Hamilton–Jacobi equation,

$$\frac{\partial S}{\partial \tau} = -\frac{(\nabla S)^2}{2m} + V + \frac{\hbar}{2m}\nabla^2 S. \tag{8}$$

Defining the momentum according to Eq. 6, the last term in Eq. 8 is interpreted as the momentum-dependent quantum potential (MDQP) [32, 51],

$$U(x,\tau) = \frac{\hbar \nabla p}{2m}, \tag{9}$$

responsible for *all* QM effects. It is non-local and influences the dynamics on equal footing with the external classical potential V. In the Lagrangian frame, Eq. 8 defines the trajectory dynamics on the inverted classical potential with MDQP of Eq. 9 added to it [32]. As a consequence, trajectories leave the region of low potential energy causing undersampling of the ground-state wavefunction at long times in high-dimensional ZPE calculations [51]. Thus, we consider the Eulerian frame-of-reference where the initial trajectory positions are stationary random grid points. In quantum trajectory dynamics, the Eulerian and Arbitrary Lagrangian-Eulerian frames were introduced by Trahan and Wyatt [52].

The trajectory momentum function at a fixed x evolves according to the gradient of Eq. 8,

$$\frac{\partial p}{\partial \tau} = -\frac{p\nabla p}{m} + \nabla(V+U). \tag{10}$$

For practical multidimensional implementation, the first and second derivatives of p in Eqs. 9 and 10 are computed approximately from the global Least Squares Fit [53] to p in the Taylor (or monomial) basis $\vec{f}$,

$$\vec{f} = (1, x, x^2 \ldots). \tag{11}$$

The fitting coefficients $\vec{c}$ minimize the difference between the exact momenta and its fit $\tilde{p}$, $\tilde{p} = \vec{f}\cdot\vec{c}$,

$$I = \langle (p-\tilde{p})^2 \rangle. \tag{12}$$

Their optimal values are the solutions to a system of linear equations $\nabla_{\vec{c}} I = \vec{0}$,

$$\mathbf{M}\vec{c} = \vec{b}, \quad \mathbf{M} = \langle \vec{f} \otimes \vec{f} \rangle, \quad \vec{b} = \langle p\vec{f} \rangle. \tag{13}$$

The expectation values are evaluated over the trajectory ensemble,

$$\langle \hat{\Omega} \rangle = \int \Omega(x)\psi^2(x,\tau)\mathrm{d}x = \sum_i \Omega(x_\tau^{(i)}) e^{-2S_\tau^{(i)}/\hbar}\delta x^{(i)}. \tag{14}$$

Superscript i labels the trajectory-related quantities after discretization of the initial wavefunction; subscript defines the time. The trajectory weight, $\delta x^{(i)}$, is the contribution of the ith trajectory to the integrals at time $\tau = 0$; the trajectory weights are constant in time.

The linear basis is exact for Gaussian wavefunctions and gives zero quantum force in Eq. 10. The quadratic basis is the smallest one that generates evolution of $p(x, \tau)$ that is different from the classical evolution. The momentum fit $\tilde{p}$ determines the approximate MDQP in Eq. 8 and in the right-hand side of Eq. 10. The latter contains the term without $\hbar$, $p\nabla p/m$, which is an approximation we have to make in the Eulerian frame in addition to approximating the MDQP terms. (In the Lagrangian frame, this term is treated exactly as part of the full-time derivative). But the advantages of the stationary points over the evolving trajectories are considerable: classical potential and its gradient is evaluated only once and, for localized ground states, the stationary points sample the high-density region of the wavefunction at all times, while in the Lagrangian formulation, the trajectories leave this region. The MDQP formulation given by Eqs. 7, 10 and 13 has been shown to give accurate ZPE estimates for anharmonic systems, including the double well, and for the triatomic molecules using the normal mode coordinates with a reasonably small (quadratic) momentum fitting. The MDQP results converged to the QM result for larger bases of 4–6 functions [32, 51].

For a system of N_{atom} atoms, the Cartesian space formulation in $3N_{\mathrm{atom}}$ dimensions has the advantage of the

simple equations of motion [23, 54] for an example of how complicated the Hamiltonian in internal coordinates is already for a non-rotating four-particle system. However, in imaginary time, the Cartesian description brings forward a question of how to treat the redundant degrees of freedom: the center-of-mass (CoM) motion and the overall rotation do not contribute to ZPE, but result in the wavefunction delocalization in the corresponding degrees of freedom. The practical, small-basis momentum fitting is accurate for localized wavefunctions close to Gaussians in Cartesian space. Therefore, wavefunction localization and shorter decay (to ZPE) time are highly desirable features for the imaginary-time approximate MDQP dynamics discussed in the remainder of this section.

2.2 The center-of-mass motion

In imaginary time, an arbitrary initial wavefunction decays to the ground state of the non-rotating system, CoM being at rest: at infinite τ, the total energy is equal to the ZPE of the internal degrees of freedom. The CoM motion is, of course, decoupled from the other modes of motion, but it can affect the accuracy of the approximate implementation. Let us examine the effect of CoM motion on the convergence of the total energy to the ZPE. We take $\psi(\vec{x},0)$ as a product of Gaussians in each Cartesian dimension centered at the minimum $\vec{x}_0$ of V,

$$\psi(x_\lambda,0)=\left(\frac{2\alpha_0^\lambda}{\pi}\right)^{1/4}\exp(-\alpha_0^\lambda(x_\lambda-x_0^\lambda)^2), \tag{15}$$

where x_0^λ and α_0^λ correspond to the dimension λ. In terms of the atomic Cartesian positions $\vec{r}_n$, for $n=1,2,\ldots,N_{\text{atom}}$ and the corresponding atomic masses, the CoM position $\vec{R}$, is

$$\vec{R}=M^{-1}\sum_n m_n\vec{r}_n,\quad M=\sum_n m_n. \tag{16}$$

Here and below the latin subscripts, i, j etc., are used to label atoms; the greek subscripts λ, μ etc., are used to index the elements of the vectors and matrices of dimensionality $3N_{\text{atom}}$. In particular,

$$\vec{x}=(\vec{r}_1,\vec{r}_2,\ldots,\vec{r}_{N_{\text{atom}}})=\{x_\lambda\},\quad \lambda=1,2,\ldots,3N_{\text{atom}}. \tag{17}$$

In full dimensionality, the masses can be arranged as an array of $3N_{\text{atom}}$ elements, $(m_1,m_1,m_1,m_2,m_2,m_2,\ldots)$.

The normalized energy of a Gaussian (for one degree of freedom) evolving according to Eq. 4 in free space is

$$E^{\text{cm}}=\frac{\alpha_0}{2M(1+2\tau\alpha_0/M)}. \tag{18}$$

The value of E^{cm} and its convergence to zero depend on α_0/M, where α_0 is large for the 'classical' degrees of freedom describing heavy particles. The convergence is hyperbolic with time and implies a complete delocalization of $\psi(x,\tau)$ in the CoM degrees of freedom. Since the approximate MDQP methodology is practical and accurate in the regime of localized wavepackets, we need to subtract CoM energy, without changing the Cartesian space wavepacket setup and Hamiltonian, and to counteract the spreading. This can be achieved by constraining—in the spirit of soft constraints used in molecular mechanics methods [55]—the CoM motion with the quadratic potential in $\vec{R}$ added to V,

$$V^{\text{cm}}=\frac{Mw^2}{2}(\vec{R}-\langle\vec{R}\rangle)^2=\frac{k_{\text{cm}}}{2}(\vec{R}-\langle\vec{R}\rangle)^2. \tag{19}$$

The average CoM position will be set to zero, $\langle\vec{R}\rangle=0$, henceforth.

Examining the imaginary-time evolution of a Gaussian in a quadratic potential [51], one finds the convergence of E^{cm} to a constant value to be exponential, which is also true for the wavepacket width parameter α_τ. Defining the coherent width $\alpha_c=Mw/2$ and $\eta=(\alpha_0-\alpha_c)/(\alpha_0+\alpha_c)$,

$$E^{\text{cm}}_{\tau\to\infty}=\frac{w}{2}\left(1+\eta^2e^{-4w\tau}\right) \tag{20}$$

$$\alpha_{\tau\to\infty}=\alpha_c\left(1+2\eta e^{-2w\tau}\right). \tag{21}$$

Obviously, presence of V^{cm} improves convergence of ZPE with time and localizes the CoM wavepacket at the coherent value. The CoM energy, which is $3w/2$ at the end of time evolution for three dimensions of $\vec{R}$, can be analytically subtracted without knowing the explicit form of the initial CoM wavefunction. For large molecular systems, $M\to\infty$, the CoM constraint might be unnecessary if α_0/M is small—the CoM wavepacket remains localized during the course of evolution—and if E^{cm} can be neglected with compared to the internal ZPE.

2.3 The overall rotation

We also need to fix the overall rotation of the molecular system and prevent delocalization of the wavefunction over the corresponding angles. This will be accomplished with the "soft constraint" as well by adding an effectively three-dimensional quadratic potential defined (after shifting CoM to zero) by three vectors $\vec{d}^{(n)}$, $n=\{1,2,3\}$, perpendicular to the average positions of all atoms $\vec{q}_i, i=1\ldots N_{\text{atom}}$, and perpendicular to the three unit vectors along the Cartesian axes $\vec{e}^{(n)}$,

$$\vec{e}^{(1)}=(1,0,0),\quad \vec{e}^{(2)}=(0,1,0),\quad \vec{e}^{(3)}=(0,0,1). \tag{22}$$

We have also used the three unit vectors along the principal axes of the moments of inertia [56] with the same effect as when using Eq. 22. Using the full dimensional vectors of average positions

$$\vec{q} = (\vec{q}_1, \vec{q}_2 \ldots \vec{q} N_{\text{atom}}) = \frac{\langle \psi | \vec{x} | \psi \rangle}{\langle \psi | \psi \rangle}, \tag{23}$$

and the three vectors defining the directions of the overall rotation (subscript i labels atoms)

$$\vec{d}_i^{(n)} = \frac{m_i}{M} \vec{q}_i \times \vec{e}^{(n)}, \vec{d}^{(n)} = (\vec{d}_1^{(n)}, \vec{d}_2^{(n)} \ldots \vec{d}_{N_{\text{atom}}}^{(n)}) \tag{24}$$

the rotational localizing potential is

$$V^{\text{rot}} = \frac{k_{\text{rot}}}{2} \sum_{n=1}^{3} \left(\vec{d}^{(n)} \cdot (\vec{x} - \vec{q}) \right)^2. \tag{25}$$

The same is more convenient when written in using matrix and vectors of full dimensionality:

$$V^{\text{rot}} = \frac{k_{\text{rot}}}{2} (\vec{x} - \vec{q}) \cdot \mathbf{D} \cdot (\vec{x} - \vec{q}), \quad D_{\lambda\mu} = \sum_{n=1}^{3} d_\lambda^{(n)} d_\mu^{(n)}. \tag{26}$$

The vectors $\vec{d}^{(n)}$ of Eq. 24 are normalized after construction. The factor m_i/M is introduced into $\vec{d}^{(n)}$ to make V^{rot} independent on the particle mass, as to have the same V^{rot} for H_2 and HD.

Since the localizing potential given by Eq. 26 is a quadratic function, the energy of the overall rotation will decay in time to the ZPE of V^{rot} defined by the three (or two for a linear molecule) non-zero eigenvalues η_μ of the mass-weighted Hessian matrix $\mathbf{h}$,

$$h_{\lambda\mu} = \frac{k_{\text{rot}} D_{\lambda\mu}}{\sqrt{m_\lambda m_\mu}}, \quad E^{\text{rot}}_{\tau\to\infty} = \frac{1}{2} \sum_{\mu=1,3} \sqrt{\eta_\mu}. \tag{27}$$

The coordinate transformation into the internal degrees of freedom is not needed [56]; the matrix size is $3N_{\text{atom}}$. Once added to $V + V^{\text{cm}}$, V^{rot} will keep the wavefunctions localized in the three directions of the overall rotation, enabling use of a cheap MDQP approximation; its analytically known contribution to the total energy should be subtracted to obtain the internal ZPE. In general, for anharmonic potentials, the rotations are not rigorously decoupled from the internal modes [57], but for the ground state, the effect of V^{rot} on ZPE is small as shown in the next section. The effects of the CoM and rotational harmonic potentials are visualized in Fig. 1 for a trimer, as described detail in the next section.

3 ZPE calculations

The vibrational energy calculations of spectroscopic accuracy for general systems are beyond the capabilities of the approximate MDQP method. This approach is not designed to compete with the exact methods, such as the Diffusion Monte Carlo or Vibrational Self-Consistent Field [58, 59] but to give cheap estimates of various types of QM effects. The ZPE calculations serve as a convenient test of the approximate MDQP, which is expected to give reasonable estimates for semi-rigid molecules by incorporating leading anharmonic terms of classical potentials.

As a proof-of-principle, we apply the formalism of Sect. 2 to compute ZPEs of systems consisting of up to $N_{\text{atom}} = 11$ nuclei with *pairwise nearest neighbor* interactions,

$$V = \sum_{i>j}^{\text{nearest}} V_{ij}, \quad V_{ij} = D(\exp(-z(r_{ij} - r_0)) - 1)^2, \tag{28}$$

where r_{ij} are the bond distances, $r_{ij} = |\vec{x}_i - \vec{x}_j|$. The mass and parameters of the Morse potential given by Eq. 28 [60] describe H_2 molecule in atomic units: $D = 0.17429$ E_h, $r_0 = 1.4$ a_0 and $z = 1.0435$ a_0^{-1}, $m = 1836$ a.u. The classical minimum energy configuration of atoms is simply the geometry when all bonds included in the sum are equal to r_0, $\langle r_{ij} \rangle = r_0$. The formalism of Sect. 2 is implemented using the quadratic fit of p. The initial wavefunction is defined as the direct product of the Gaussians (15) centered at the minimum of the classical potential. The width parameters α_0 were assigned the same values for all dimensions and did not correspond to the normal mode values. The sampling of the random grid points is uniform [53] within the region of the wavefunction density $\psi^2(x, 0) > 10^{-\varepsilon}$. Parameter ε is the sampling cutoff in a single dimension. To make the low-order polynomial fitting accurate, only the central region, $\varepsilon = 0.125$, is typically sampled. The force constants in Eqs. 19 and 26 are chosen to give energy due to the localization potentials, Eqs. 19 and 26, on the order of the internal ZPE. The time evolution of S and p in the Eulerian frame-of-reference according to Eqs. 8 and 10 is implemented in a straightforward manner giving linear convergence of the wavefunction norm and (unnormalized) energy with respect to the time step. (i) The polynomial fit, $\tilde{p}$, of the function $p(x)$ is used in the right-hand side (RHS) of Eqs. 8 and 10. (ii) The values of S and p are incremented by the corresponding RHS values multiplied by $d\tau$. This choice allows the RHS of Eq. 10 to be an analytical gradient of Eq. 8 throughout the propagation.

3.1 A diatomic molecule

H_2 molecule is described in six Cartesian coordinates with positions of protons 1 and 2 denoted as $\vec{r}_1 = (x_1, x_2, x_3)$ and $\vec{r}_2 = (x_4, x_5, x_6)$. The initial width parameter is $\alpha_0 = 12$ a_0^{-2} in all dimensions; the molecule is oriented along the z-axis, and its CoM is at zero. The value of α_0 is roughly defined by the normal mode frequencies, but as shown in [32] in practice, the ZPE is rather insensitive to this choice. In the Cartesian coordinates, the localizing CoM potential is

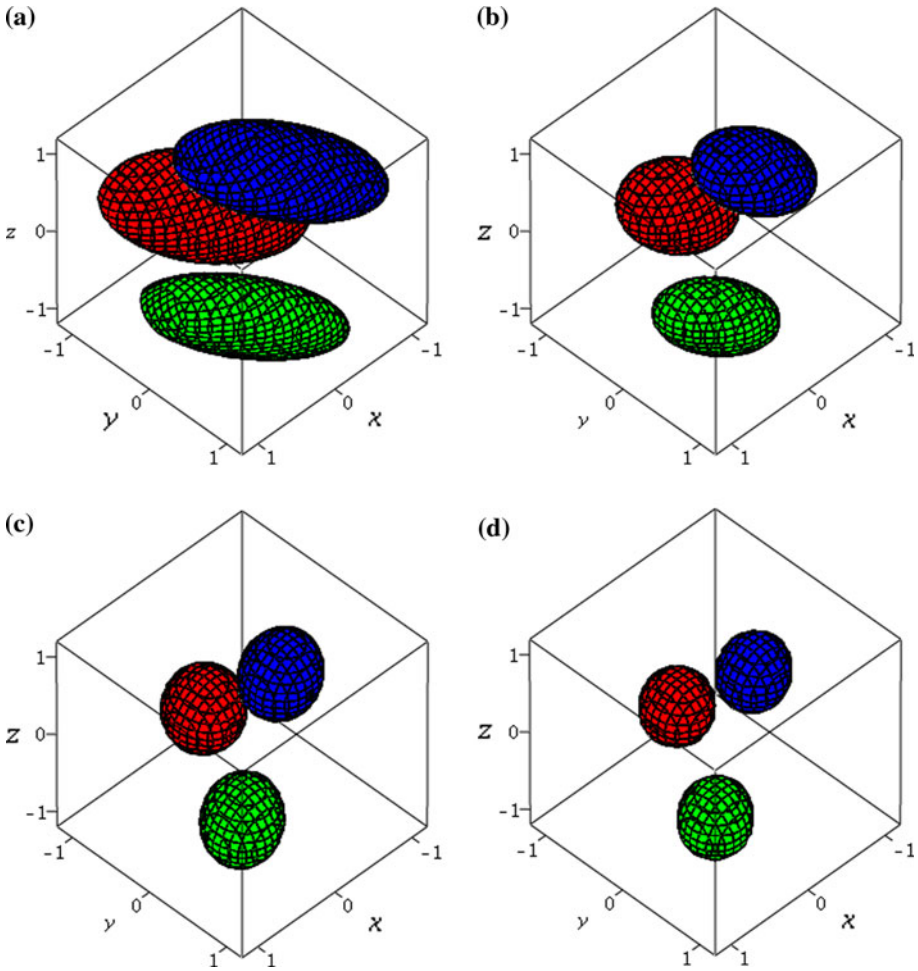

Fig. 1 Trimer: density localization with and without constraints. The isodensity surfaces are shown after evolution up to $\tau = 0.1$ a.u. **a** without localization potentials, **b** with just V^{cm} included, **c** with just V^{rot} included and **d** with both CoM and overall rotation localizing potentials included

$$V^{\mathrm{cm}} = \frac{k_{\mathrm{cm}}}{8}\left((x_1 + x_4)^2 + (x_2 + x_5)^2 + (x_3 + x_6)^2\right). \tag{29}$$

The rotational potential is

$$V^{\mathrm{rot}} = \frac{k_{\mathrm{rot}}}{4}\left((x_1 - x_4)^2 + (x_2 - x_5)^2\right), \tag{30}$$

which makes physical sense—rotations from the original z-direction will increase the total energy. Figure 2 shows the total normalized energy of the wavefunction with the ZPEs of localizing potentials subtracted as appropriate. The values of the force constants were the same $k_{\mathrm{cm}} = k_{\mathrm{rot}} = 1.5\mathrm{E}_{h/a}\,\frac{2}{0}$, which gave ZPEs of 2.86 E_0 and 3.04 E_0, respectively. E_0 is the analytical ZPE of the Morse potential, $E_0 = 1.00187 \times 10^{-2}$ E_h. The trajectory ensemble consisted of 2500 random points uniformly sampling the initial density within the cutoff parameter $\varepsilon = 0.125$. The momentum components were fitted with quadratic polynomials yielding the total basis size of $N_{\mathrm{bas}} = 28$. The scaling of the quadratic basis with the dimensionality is $N_{\mathrm{bas}} = (N_d + 1)(N_{\mathrm{d}} + 2)/2$, $N_{\mathrm{d}} = 3N_{\mathrm{atom}}$. The approximate MDQP evolution is cheap: propagation of 1,000 trajectories for one thousand time steps in six

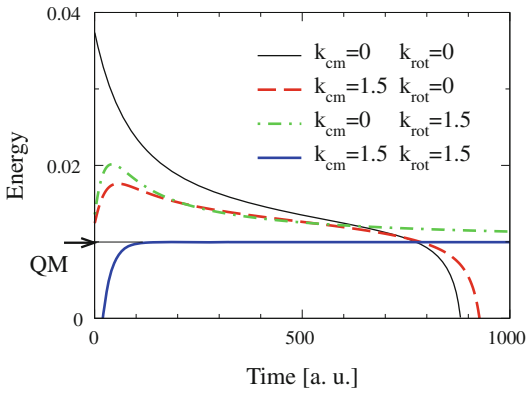

Fig. 2 The internal energy of the H_2 system computed in 6D Cartesian coordinates. The force constants of the confining potentials are on the legend. *Arrow marks* the analytical internal ZPE

dimensions takes about 2 s on a desktop workstation. The scaling of CPU is linear with respect to the number of trajectories and quadratic with respect to the basis size.

As seen from Fig. 2 without V^{rot}, the wavepacket energy E sharply drops after $\tau \approx$ 700 a.u., because the wavefunction spread in angles makes the quadratic momentum

Table 1 The zero-point energy for H_2 (and isotope substitutions) computed from imaginary-time propagation in 6 Cartesian coordinates

N_{traj}	t (a.u.)	m (a.u.)	α_0 (a_0^{-2})	$E(\tau)$ (%)	$dE/d\tau$, (E_h/a.u.)
100	250	HH	12	99.60	1.9×10^{-8}
500	250	HH	12	99.52	2.5×10^{-8}
2500	250	HH	12	99.52	2.3×10^{-8}
2500	250	HH	9	99.36	7.2×10^{-9}
2500	250	HH	18	99.70	6.0×10^{-8}
2500	250	HD	12	99.73	-6.6×10^{-8}
2500	250	DD	12	99.61	-3.2×10^{-7}
2500	250	HT	12	99.68	-2.1×10^{-7}
2500	250	DT	12	99.43	-5.8×10^{-7}
2500*	250	HH	12	98.05	9.6×10^{-7}

All calculations were performed with the quadratic momentum fitting, except for the last calculation marked * performed with the linear momentum fitting

fitting inaccurate. With the rotational localizing potential in place, the energy converges to a constant, but it does so slowly without the CoM constraint. The accuracy of the internal ZPEs is given in Table 1. The initial orientation of H_2 was along the z-axis, but to verify the invariance of the formalism to rotation, the initial orientation for the isotopically substituted species was rotated. The initial Gaussian wavefunction was centered at $\vec{x}_0 = (0.73654, -0.40656, 0.40415, -0.36827, 0.20328, -0.20207)$ a_0. V^{rot} was constructed using the principal axes of inertia rather than Cartesian directions of Eq. 22 in this case. The internal ZPE is given as percent of the analytical ZPE. The accuracy is within 0.5% in all cases. The linear fitting of the momentum gives ZPE within 2% and, more importantly, does not converge to a plateau value with time.

3.2 Clusters

First, we will examine the trimer with pairwise interactions via the Morse potential described above. The exact QM ZPEs are obtained from the Fourier-transforms of autocorrelation functions propagated in real time using the split-operator method [61]. The system was described in three dimensions in the Jacobi coordinates at zero total angular momentum using a grid of 32×32 points in the radial coordinates and 25 Discrete Variable Representation (Gauss-Legendre) points in angle [10]. The energy level resolution is 4×10^{-5} E_h. For the MDQP calculation, the parameters are $\varepsilon = 0.125$, $k_{cm} = k_{rot} = 8$ E_h/a_0^2. Ensemble of 2500 trajectories was evolved up to $\tau = 200$ a.u. The initial width parameter is taken $\alpha_0 = 12$ a_0^{-2} for all 9 Cartesian dimensions. The centers of the Gaussians form an equilateral triangle in xy-plane with the side of $r_0 = 1.4$ a_0. This configuration gives the lowest value of the

Table 2 ZPE for the hydrogen (and deuterium substituted) model trimer computed from imaginary-time propagation in 9 Cartesian coordinates

Species	$E(\tau)$ (E_h)	$dE/d\tau$ (E_h/a.u.)	E^{QM}	$E(\tau)/E^{QM}$
H_3	0.029496	3.0×10^{-8}	0.029368	1.0044
H_2D	0.026880	-1.0×10^{-7}	0.026777	1.0039
HD_2	0.024026	-4.5×10^{-7}	0.023950	1.0039
D_3	0.020929	-1.0×10^{-6}	0.020887	1.0020

The number of trajectories is 2500, final $\tau = 200$ a.u., $\varepsilon = 0.125$ and $\alpha_0 = 12$ a_0^{-2} for all systems

classical potential. The internal ZPEs, given in Table 2, are computed for H_3 and for the deuterium substituted species and compared to the exact QM results. As seen from the table, the MDQP with quadratic fitting gives accuracy better than 0.4% and converges to the plateau value within 10^{-6} E_h. This shows that the choice of the rotational localization potential of Eq. 26 is correct. The MDQP calculation takes 6 s, whereas the exact QM propagation (using a fairly small grid described above) takes about 6 min.

There are two parameters that determine the accuracy of the MDQP calculation: the force constants of the localization potentials, k_{cm} and k_{rot} and the cutoff parameter ε. (The fitting basis size, obviously, has crucial effect on the accuracy, but due to polynomial scaling of the basis size with N_{atom}, we consider only the quadratic basis). The CoM motion separates from other modes of motion; the rotational motion is separable if the classical potential is quadratic. In this case, considering for simplicity $k_{cm} = k_{rot} = k$, the energy associated with the added localization potentials given by Eqs. 19 and 26 is a linear function of $\sqrt{k}$. Once this localization energy is subtracted from the total energy, the remaining internal modes ZPE should be constant. Figure 3 shows the internal modes ZPE for H_3 extracted from calculations with various localization force constant k. As seen from the plot, indeed there is a

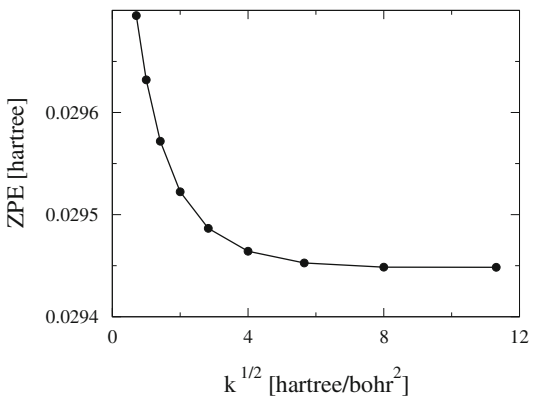

Fig. 3 Dependence of the internal ZPE on the force constant of the localization potentials given by Eqs. 19 and 26 for the trimer; $k_{cm} = k_{rot} = k$

regime of k, where the internal ZPE approaches a plateau value (which corresponds to the total ZPE being linear in $\sqrt{k}$) yielding the internal ZPE estimates.

The effect of localization in CoM and rotation modes is visualized on Fig. 1. The isodensity surface plotted on the figure at $\tau = 200$ a.u. is approximated with three-dimensional Gaussian functions for each atom using single-particle fitting of $\vec{p}$. Panel (a) has zero V^{cm} and V^{rot}; on panel (b), the CoM localization is introduced; on panel (c), just the rotational localization is included. Both, V^{rot} and V^{cm}, were included on panel (d). The value of the force constant is $k = 2$. As we see, V^{rot} and V^{cm} are essential for localization of the wavepacket. The effect of V^{cm} is not as dramatic as that for Vrot. As discussed in Sect. 2, V^{cm} accelerates convergence of the total energy to a plateau value.

The dependence of ZPE on the sampling cutoff parameter ε is illustrated on Fig. 4. The initial random points sample the region of the wavefunction density where $\rho > 10^{-\varepsilon}$ for each dimension. Sampling more compact region of space—smaller ε values—improves accuracy of the fitting, but making ε too small looses information on the anharmonicity of the potential. On the figure, the ZPE is shown for the linear and quadratic fitting of the momentum: the linear fit approaches the normal mode value as $\varepsilon \to 0$; the quadratic fit approaches a value about 0.3% lower than the exact QM result. The normal mode estimate is 1.9% higher. The MDQP accuracy is worse for large values of ε. This difference of 0.3% is the limit of the quadratic fitting basis. The parameter values $k = 8$, $\varepsilon = 0.125$ and the quadratic fitting basis will be used for larges systems below unless stated otherwise.

To test the scalability of the approximate MDQP, we extend our model system to clusters of up to 11 atoms.

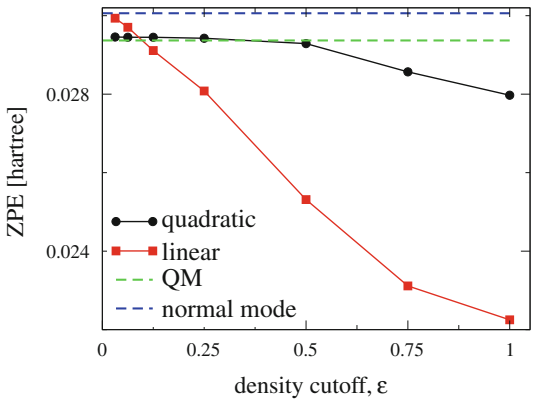

Fig. 4 Dependence of the ZPE of the trimer on the sampling cutoff parameter ε, $\rho > 10^{-\varepsilon}$. The results for the linear momentum fitting converge to the normal mode ZPE; the results for the quadratic momentum fitting the QM result

The cluster geometries are obtained by first adding an atom on the positive z-axis above the trimer in xy-plane to create a tetrahedron (tetramer), then adding the fifth atom on the negative z-axis (pentamer). More atoms are added atop of each face of the pentamer creating an hexagonal close-packed array. The initial parameters are $\alpha_0 = 12$ a_0^{-2}, $\varepsilon = 0.125$. Ensembles of $N_{\mathrm{traj}} = 2500$ trajectories were evolved up to $\tau = 200$ a.u. At this time, the normalized energies reached plateau values, which are the MDQP estimates of the cluster ZPEs. These values are compared to the normal mode ZPEs in Table 3 for $N_{\mathrm{atom}} = 3 - 8, 11$. The time derivatives, $dE(\tau)/d\tau$, indicate the convergence. The results are converged with respect to the number of trajectories within 4 digits and with respect to ε within 0.5%. Figure 5a shows the ZPEs per bond in the units of the energy of the dimer bond. The difference between the MDQP estimates and normal mode estimates changes from 2% for 3 bonds to 0.5% for 27 bonds. For the trimer, for which we have accurate QM ZPE, the difference between the QM and MDQP result is 6 times smaller than between the MDQP and the normal mode estimate. Thus, MDQP calculation captures changes in the ZPE due to anharmonicity of the Morse potentials. Note that the leading, cubic, anharmonic term gives zero correction to the energy within the first-order perturbation theory. This claim is consistent with the ZPE calculation for particles that are 10 times heavier, $m = 18360$ a.u. The results are shown on Fig. 5b. For heavier particles, the eigenstates are more localized. Therefore, the normal mode approximation is more accurate, and indeed, the discrepancy between the MDQP and normal mode approximations is smaller ($\approx$ 3 times smaller since the energy scales as $m^{-1/2}$). Compared to $m = 1836$ a.u. calculations, the initial width was changed to $\alpha_0 = 38$ a_0^{-2} and the evolution was performed up to $\tau = 1{,}000$ a.u.

Table 3 Internal energy for the clusters, $E(\tau)$, approaching the ZPE at $\tau = 200$ a.u., computed from the imaginary-time MDQP propagation in Cartesian coordinates

N_{atom}	N_{bond}	$E(\tau)$ (E_h)	$dE/d\tau$ (E_h/a.u.)	E^{norm}
3	3	0.02947	-0.81×10^{-9}	0.03006
4	6	0.05833	-0.26×10^{-8}	0.05926
5	9	0.08665	0.29×10^{-9}	0.08780
6	12	0.11470	0.66×10^{-8}	0.11597
7	15	0.14245	0.15×10^{-7}	0.14378
8	18	0.16977	0.25×10^{-7}	0.17123
11	27	0.24962	0.55×10^{-7}	0.25115

The last column contains the normal mode ZPE estimates. The parameters of calculations are described in text

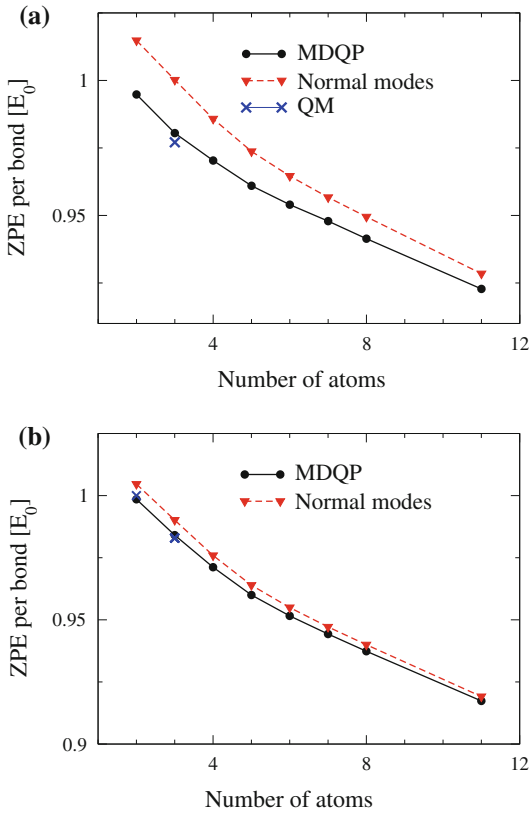

Fig. 5 ZPE per bond obtained form the approximate MDQP evolution and in the normal mode approximation for atomic masses $m = 1836$ a.u. on panel (a) and $m = 18360$ a.u. on panel (b). The energy values are given in the units of the single bond energy of the Morse oscillator, E_0

4 Discussion and summary

We have presented an approximate approach to the wavepacket evolution in imaginary time in Cartesian coordinates and demonstrated its efficiency for high-dimensional systems. The trajectory formulation of the QM diffusion equation 4 allows one to express all the quantum effects through a single non-local potential-like term—the momentum-dependent quantum potential (MDQP). The quantum potential and the corresponding force are determined from the global Least Squares Fit of the momentum, which gives polynomial scaling with the number of dimensions to the method. For the quadratic fitting of the momenta, the number of basis functions scales quadratically with the dimensionality; the scaling of the overall numerical cost is dominated by the classical trajectory evolution, which is linear. The trajectory formulation itself allows random sampling of the initial wavefunction density, thus avoiding the exponential scaling with dimensionality of the wavefunction representation typical for the exact QM methods.

The approximate MDQP approach has been implemented in the Eulerian frame-of-reference and used for ZPE calculations. The Eulerian formulation necessitates approximation of the term, $\nabla\, p/m$, that does not vanish in the classical limit of $\hbar \to 0$, but it has two important practical advantages over the Lagrangian formulation with moving trajectories, at least for the potentials with localized minima: (i) the evolution equations in the Eulerian formulation are solved for stationary points—thus the representation of the ground state does not deteriorate with time; (ii) the classical potential and its gradient has to be computed only once—a tremendous saving for on-the-fly dynamics. In the ZPE calculations performed, we were able to use small ensembles of 2500 points for all cluster sizes, fairly localized around the minimum of V, due to the special feature of the quantum imaginary-time trajectories: the energy of each trajectory becomes equal to the ZPE as evolution unfolds. Such ensembles will be too small to represent the entire ground state, though the Gaussian approximation to it can be easily constructed. For systems with delocalized ground states or multiple minima of V, some combination of the Eulerian/Lagrangian formulation [48] or treatment of multiple low-energy regions as separate domains may be required. Such treatments will be more expensive requiring more trajectories and/or higher order fitting bases.

Implementation in Cartesian space is important because this is the framework of the classical mechanics methods, such as molecular dynamics, equations of motion and Hamiltonians take the simplest form, and because such formulation naturally invites mixed quantum/classical description of the nuclei. In order to include the QM correction on dynamics in Cartesian coordinates, we have introduced additional potentials that keep the wavefunction localized in the CoM and overall rotation degrees of freedom. This localization is necessary for accurate determination of MDQP in Cartesian coordinates within the minimal, quadratic basis. We have shown that there is a range of the force constants for the localizing potentials, where their effect on the internal ZPE is small and can be analytically subtracted from the total energy. The normal mode analysis can guide the choice of these parameters, as well as of the initial wavepacket widths. The concept of localizing potentials is similar to the soft constraint of molecular mechanics. For large molecular systems, they may become irrelevant, as it takes longer for a large system to move or rotate as a whole. The energy associated with the localization of the initial wavefunction in these degrees of freedom will be small compared to the internal ZPE and can be estimated from the diagonalization of the Hessian in Cartesian coordinates. Alternatively, one can consider constraining the overall motion and rotation by projection of the forces on the undesired directions, something that

will be explored in the future. Application of the quadratic potential in the CoM coordinates should speed up the convergence to the ground state regardless of the propagation method.

So far, we conclude that the cost and scalability of the quadratic fitting for systems with localized ground state is promising. Cheap MDQP calculations give reasonable corrections to the normal mode ZPE estimates. The Cartesian coordinates implementation is compatible with classical simulation methods. The ultimate goal of this research is inclusion of QM corrections on dynamics of nuclei in large molecular systems. Future work will include thermal reaction rate calculations using the quantum trajectories in imaginary and real time and the mixed quantum/classical treatment of nuclei.

Acknowledgments This material is based on work partially supported by the South Carolina Research foundation and by the National Science Foundation under Grant No. CHE-1056188. The author is grateful to V. A. Rassolov for many stimulating discussions.

References

1. Czako G, Bowman JM (2009) J Chem Phys 131
2. Zhang W, Kawamata H, Liu K (2009) Science 325:303
3. Dekker C, Ratner MA (2001) Phys World 14:29
4. Lear JD, Wasserman ZR, DeGrado WF (1988) Science 240:1177
5. Cha Y, Murray CJ, Klinman JP (1989) Science 243:1325
6. Knapp MJ, Klinman JP (2002) Eur J of Biochem 269:3113
7. Prezhdo OV, Rossky PJ (1997) J Chem Phys 107:5863
8. Brooksby C, Prezhdo O, Reid P (2003) J Chem Phys 119:9111
9. Prezhdo OV, Duncan WR, Prezhdo VV (2008) Acc Chem Res 41:339
10. Light JC, Carrington T Jr (2000) Adv Chem Phys 114:263
11. Meyer HD, Manthe U, Cederbaum LS (1990) Chem Phys Lett 165:73
12. Meyer HD, Worth GA (2003) Theor Chem Acc 109:251
13. Wang HB, Thoss M (2003) J Chem Phys 119:1289
14. Shalashilin DV, Child MS (2004) J Chem Phys 121:3563
15. Wu YH, Batista VS (2006) J Chem Phys 124:224305
16. Ben-Nun M, Quenneville J, Martinez TJ (2001) J Chem Phys 104:5161
17. Kim SY, Hammes-Schiffer S (2006) J Chem Phys 124:244102
18. Prezhdo O, Kisil V (1997) Phys Rev A 56:162
19. Hone TD, Izvekov S, Voth GA (2005) J Chem Phys 122:054105
20. Gao J, Truhlar DG (2002) Annu Rev Phys Chem 53:467
21. Náray-Szabó, G, Warshel, A (eds) (1997) Computational approaches to biochemical reactivity, vol. 19 of Understanding chemical reactivity. Kluwer Academic Publishers, Dordrecht
22. Gindensperger E, Meier C, Beswick JA (2000) J Chem Phys 113:9369
23. Meier C, Manthe U (2001) J Chem Phys 115:5477
24. Karplus M, Sharma RD, Porter RN (1964) J Chem Phys 40:2033
25. Rassolov VA, Garashchuk S (2008) Chem Phys Lett 464:262
26. Schatz GC, Bowman JM, Kuppermann A (1975) J Chem Phys 63:685
27. Miller WH (2001) J Phys Chem A 105:2942
28. Wyatt RE (2005) Quantum dynamics with trajectories: introduction to quantum hydrodynamics. Springer, New York
29. Madelung E (1927) Z Phys 40:322
30. de Broglie L (1930) An introduction to the study ot wave mechanics. E. P. Dutton and Company Inc., New York
31. Bohm D (1952) Phys Rev 85:166
32. Garashchuk S (2010) J. Chem. Phys. 132:014112
33. Garashchuk S, Rassolov V, Prezhdo O (2011) Reviews in computational chemistry, vol 27, chap. Semiclassical Bohmian dynamics. Wiley, Hoboken, pp 111–210
34. Ramond P (1990) Field theory: a modern primer. Addison-Wesley, Reading
35. Feynman RP, Hibbs AR (1965) Quantum mechanics and path integrals. McGraw-Hill, New York
36. Frantsuzov PA and Mandelshtam VA (2008) J Chem Phys 128
37. Chen X, Wu YH, Batista VS (2005) J Chem Phys 122
38. Cartarius H and Pollak E (2011) J Chem Phys 134
39. Miller WH (1971) J Chem Phys 55:3146
40. Blume D, Lewerenz M, Niyaz P, Whaley KB (1997) Phys Rev E 55:3664
41. Ceperley DM, Mitas L (1996) Advances in chemical physics, chap. Monte Carlo methods in quantum chemistry. Wiley, London
42. Lester WA Jr, Mitas L, Hammond B (2009) Chem Phys Lett 478:1
43. Viel A, Coutinho-Neto MD, Manthe U (2007) J Chem Phys 126:024308
44. Hinkle CE, McCoy AB (2008) J Phys Chem A 112:2058
45. Miller WH, Schwartz SD, Tromp JW (1983) J Chem Phys 79:4889
46. Rassolov VA, Garashchuk S, Schatz GC (2006) J Phys Chem. A 110:5530
47. Garashchuk S, Vazhappilly T (2010) J Phys Chem C 114:20595
48. Garashchuk S, Mazzuca J, Vazhappilly T (2011b) J Chem Phys 135:034104
49. Liu J, Makri N (2005) Mol Phys 103:1083
50. Goldfarb Y, Degani I, Tannor DJ (2007) Chem Phys 338:106
51. Garashchuk S (2010b) Chem Phys Lett 491:96
52. Trahan CJ, Wyatt RE (2003) J Chem Phys 118:4784
53. Press WH, Flannery BP, Teukolsky SA, Vetterling WT (1992) Numerical recipes: the art of scientific computing. 2nd edn. Cambridge University Press, Cambridge
54. Reed SK, González-Martínez ML, Rubayo-Soneira J, and Shalashilin DV (2011) J Chem Phys 134
55. Dubbeldam D, Oxford GAE, Krishna R, Broadbelt LJ, and Snurr RQ (2010) J Chem Phys 133
56. Ochterski JW (1999) Vibrational analysis in Gaussian, http://www.gaussian.com/g_-whitepap/vib.htm
57. Meyer H (2002) Annu Rev Phys Chem 53:141
58. M. A. Ratner, Gerber RB (1986) J Phys Chem 90:20
59. Carter S, Culik SJ, Bowman JM (1997) J Chem Phys 107:10458
60. Morse PM (1929) Phys Rev 34:57
61. Feit MD, Fleck JA Jr, Steiger A (1982) J Comp Phys 47:412